Angle Closure Glaucoma Detection using Fractal Dimension Index on SS-OCT images

Soe Ni Ni[1], Pina Marziliano1[1] and Hon- Tym Wong[2]

Abstract— **Optical coherence tomography (OCT) is a high resolution, rapid and non-invasive screening tool for angle closure glaucoma. In this paper, we propose a new strategy for automatic and landmark invariant quantification of the anterior chamber angle of the eye using swept source optical coherence tomography (SS-OCT) images. Seven hundred and eight swept source optical coherence tomography SS-OCT images from 148 patients with average age of (59.48 $\pm$ 8.97) were analyzed in this study. The angle structure is measured by fractal dimension (FD) analysis to quantify the complexity or changes of angle recess. We evaluated the FD index with biometric parameters for classification of open angle and angle closure glaucoma. The proposed fractal dimension index gives a better representation of the angle configuration for capturing the nature of the angle dynamics involved in different forms of open and closed angle glaucoma (average FD (standard deviation): 1.944 (0.045) for open and 1.894 (0.043) for closed angle). It showed that the proposed approach has promising potential to become a computer aided diagnostic tool for angle closure glaucoma (ACG) disease.**

I. INTRODUCTION

Glaucoma is the second leading cause of blindness [1]. Many glaucoma tests are time consuming and require trained personal as well as special equipment. Recent advances in computer-based systems improved the glaucoma screening process. The imaging of angle between the iris and the cornea is the key for open and angle closure glaucoma (ACG) diagnosis. Early detection of ACG using imaging technology has recently gained much clinical interest and is important for preventing irreversible blindness.

Gonioscopy, which was introduced by Trantas in 1899 [2], has been considered as the gold standard technique to assess the iridocorneal angle structure qualitatively for every glaucoma patient. However, quantification of measurements is unreliable since it is subjective and dependent on the operator.

Meanwhile, imaging technology has recently received much attention in clinical interest for early detection of ACG. OCT is a high resolution, rapid and non-invasive screening tool for angle closure glaucoma and its technology has evolved rapidly from time-domain to spectral-domain. Swept source OCT (Casia SS-1000) is a newly developed novel imaging technology which provides a detailed examination of the structures of anterior chamber angle (ACA) [3].

In recent years, much research have been investigating in angle closure glaucoma detection based on OCT imaging modalities. However, the angle assessment, e.g. angle opening distance (AOD500) [4], is generally based on the manual or automatic detection of scleral spur (SS), which is not identifiable in 20% to 30% of the Visante OCT images [5].

To cope with the problem of identifying the scleral spur, Schwalbes line (SL) was proposed as a novel landmark which could be manually detected in more than 90% of Cirrus HD-OCT images [5]. Tian et al. [6] developed an automatic algorithm to detect SL in HD-OCT images and to measure the angle recess parameters based on Schwalbe's line. However, the existing methods use a single distance or area for measurement of iridocorneal angle, without consideration of the whole angle profile. Cheung et.al [7] showed that the Schwalbe's line based AOD measurement is inaccurate due to the irregular iris surface.

Therefore, our previous study [8] proposed two new parameters, mAOD and AT_{sl}, based on the continuous AOD to assess the anterior chamber angle. These two new parameters tried to overcome the limitations in the single measurement of AOD when the iris surface is irregular and the angle is more occludable [7].

However, all the previous studies were based on gonioscopic ground truth data in classification which is very subjective and time consuming. ACA classification is a challenging task since there are intermediate cases that are difficult to classify as open angle or closed angle using the same clinical features such as angle assessment and gonioscopic grading even for human experts as in Fig. 1. Based on image classification experience, using only one or two dimensional clinical features is insufficient to achieve good performance [9]. Alternative ideas and novel solutions are still needed for screening and diagnosis of angle closure glaucoma.

Hence, Xu et. al [9]-[10] proposed to classify the glaucoma subtype by visual image quality based on histograms of oriented gradients (HOG) features and histogram equalized pixel (HEP) values. They achieved 75.8% $\pm$ 6.4% and 84.0% $\pm$ 5.7% balanced accuracy with 85% specificity to identify glaucoma subtype in OCT images.

Another fact to note is that ACA anatomy is complex and irregular in shape. The complexity or changes of the

*This work was supported by a Translational Clinical Research Partnership grant from the Biomedical Research Council (BMRC), A*Star, Singapore.

S. Ni Ni is with the School of Electrical and Electronic Engineering, Nanyang Technological University, Singapore. (e-mail: ninisoe@ntu.edu.sg.

P. Marziliano is an Associate Professor in the Division of Information Engineering, School of Electrical and Electronic Engineering, Nanyang Technological University, Singapore. (e-mail: epina@ntu.edu.sg).

H.-T.Wong is with the Department of Ophthalmology, Tan Tock Seng Hospital,Singapore, and with the National Healthcare Group Eye Institute, Singapore. (e-mail: Hon_Tym_Wong@ttsh.com.sg).

978-1-4244-7929-0/14/$26.00 ©2014 IEEE

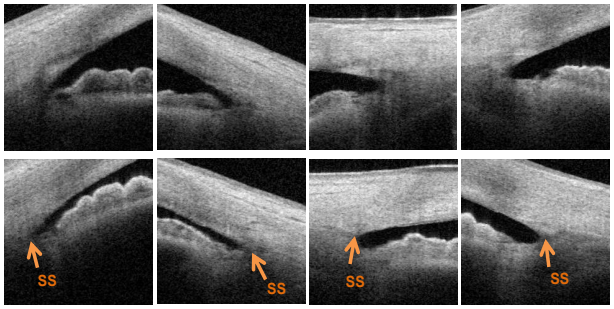

Fig. 1. ACA classification on HD SS-OCT images. The ACAs in the top row are clinically labeled as closed angle and the ACAs in the lower row are labelled as open angle.

iridocorneal angle can be measured quantitatively and qualitatively with shape descriptors. Moreover, the shape analysis might give more freedom in computation and is less sensitive to the accurate detection of the landmarks-the Scleral spur (SS) and the Schwalbe's line (SL). Using this approach, the shape analysis may be successfully applied both quantitatively and objectively to characterize angle shape of anterior chamber of SS-OCT images as a new index for ACG diagnosis.

To overcome some challenges faced by the above angle assessment techniques, we explore fractal analysis. The concept of fractal dimension (FD) is useful in the measurement, analysis, and classification of shape and texture. The complex and erratic shape description in terms of self-similarity was introduced by Mandelbrot [11]. However, although FD has been used extensively in characterizing self-affinity in various kinds of biomedical research, little attention has been paid in automated glaucoma subtype classification using the feasibility of fractal and multifaractal theory on retinal nerve fiber layer (RNFL) and optic disc [12].

This paper presents a novel diagnostic strategy to develop quantitative index of the iridocorneal angle for glaucoma detection using the morphological fractal shape analysis on SS-OCT images.

The rest of this paper is organized as follows: Section II describes the overview of the framework for pre-processing, segmentation of anterior chamber angle, region of interest (ROI) detection and fractal dimension analysis of angle closure glaucoma. The experiments and results are presented in Section III. Finally section IV concludes the paper with the future work.

II. Methods

The architecture of the overall proposed system is shown in Fig. 2. It mainly consists of three steps, pre-processing, segmentation of anterior chamber and fractal dimension analysis.

The original image denoted by $I(x,y)$, is first pre-processed to remove the vertical saturation artifacts as in [8] and the processed image is denoted by $\hat{I}(x,y)$, where $(x,y) \in [1,M] \times [1,N]$ are the pixels coordinates and $M \times N$

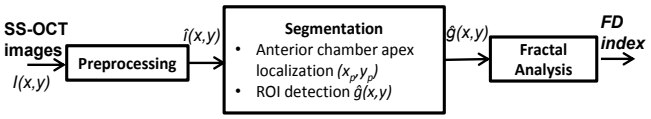

Fig. 2. Overview of the automatic classification system for open angle and angle closure glaucoma using SS-OCT images

is the size of the image. We firstly performed pre-processing steps as the method in our previous study [8]. Then $\hat{I}(x,y)$ is segmented to detect the cornea, the iris and the anterior chamber. The anterior chamber angle apex is localized and we detect the ROI for further feature extraction afterwards. Lastly, the fractal dimension (FD) index is calculated to quantify the anterior chamber. The details of each step are presented in the following sections.

A. Segmentation of Anterior Chamber

After removing the vertical saturation artifacts, the segmentation was performed in the SS-OCT images. The anterior chamber, the cornea, the iris, and their edges are extracted by image segmentation method as in Tian et. al. [6]. First, we convert the artifact removal SS-OCT image $\hat{I}(x,y)$ of dimension $M \times N$ to a binary image defined by Eq. (1)

$$g(x,y) = \begin{cases} 1 & \text{if } \hat{I}(x,y) > \text{threshold}, \\ 0 & \text{otherwise} \end{cases} \quad (1)$$

where the threshold can be calculated by Otsu's method [13], in which the intra class variance is minimized and the inter class variance is maximized. The cornea and the iris can be separated by the connected component labeling and morphological image processing method. The basic idea of this method is to scan the image and group its pixels into components based on connectivity and assign each component with a unique label. The anterior chamber (AC) is identified as the M_{AC}. The upper and lower boundaries of AC are the lower boundary of the cornea (E_e) and inner boundary of the iris (E_i).

B. ACA apex localization and ROI detection

After the extraction of the lower cornea (E_e), the upper iris (E_i) and the anterior chamber, we localized the ACA apex (x_p, y_p) point which is the end point of E_e. In [9], the authors localized the ACA vertex by two observations such as, single ACA and multiple ACA. In our case, we could get only single ACA because of the improvement of the segmentation and preprocessing steps. Consequently, we could clearly localize the ACA apex as shown in Fig. 3. The algorithm could determine the exact location of the apex point of the anterior chamber region for efficient angle calculation. It is highly imperative to detect Glaucoma in its early stages for diagnosis.

For ROI detection in OCT images, we selected the ACA region which includes SS and SL based on the ACA apex point (x_p, y_p) since the ACA is between the cornea and the iris as shown in Fig. 3. A region of interest (ROI) image

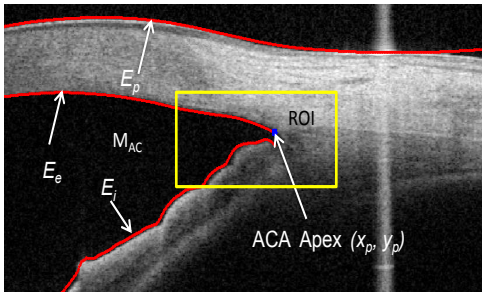

Fig. 3. The segmentation of the upper boundary of cornea (E_p), the lower boundary of cornea (E_e), the upper boundary of iris (E_i), segmentation of anterior chamber M_{AC}, localization of the ACA apex point (x_p, y_p) and the yellow bounding box for ROI detection

is defined in Eq. (2) by $\hat{g}(x,y)$ where $(x,y) \in [1,m] \times [1,n]$ are the pixels coordinates and $m \times n$ is the size of the ROI image. It is cropped out from the original image for nasal and temporal quadrant according to the following Eq. (2)

$$\hat{g}(x,y) = \{(x,y)|I(x,y), \\ (x,y) \in [x_p - 150, x_p + 100] \times [y_p - 50, y_p + 50]\}. \quad (2)$$

The ROI is formed by 150 pixels to the left, 100 pixels to the right of Apex point (x_p) in the horizontal axis and 50 pixels to the top and bottom from the apex point (y_p) in the vertical axis. The ROI image has [250 × 100] pixels. If the image is the nasal scan of the left eye or the temporal scan of the right eye, we need to flip the horizontal position of the ROI images. The segmented ACA, the edges of the cornea, the upper iris and detected ROI are illustrated in Fig.3.

C. Fractal Analysis of ACA

The fractal dimension for 2D gray level images quantified by differential box counting method (DBCM) was proposed by Sarkar et.al [14]. We utilized the fractal complex analysis on the selected ROI region of iridocorneal angle image denoted by $\hat{g}(x,y)$.

For each pixel (x,y) in the $\hat{g}(x,y)$ image, we compute the fractal dimension of a small window W surrounding the pixel (x,y). We assigned this fractal dimension to that pixel (x,y). We divide W into $(\frac{1}{r})^2$. DBC presumes that the image belongs to a 3D space $z = \hat{g}(x,y)$, where (x,y) denotes the two-dimensional positions and z denotes the gray level of the image. The image with size $m \times n$ was scaled down by boxes with size $r \times r \times h$ to many overlapping grids. If the total number of gray levels is G then

$$\frac{G}{h} = \frac{m}{r} \quad (3)$$

where r refers to the compressibility factor, h indicates the height of the box and G denotes the range of the gray level in one grid. Supposing that the maximum and the minimum gray values of the image in pixel $(x,y)th$ grid fall in the box numbers lth and kth box respectively, $n_r(x,y) = l - k + 1$ denotes the number of needed boxes to cover the grid. Taking contribution from all grids, we have

$$\bar{N}_r = \sum n_r(x,y). \quad (4)$$

The value of $\bar{N}_r$ is determined by the different values of box sizes r. After selecting different values of r and finding $\bar{N}_r$, the fractal dimension FD can be obtained by the following Eq. (5)

$$\text{FD} = \frac{log(\bar{N}_r)}{log(\frac{1}{r})}. \quad (5)$$

III. Experiments and Results

In this research, we recruited 148 subjects (90 females and 58 males) with average age of 59.48 ± 8.97 from the glaucoma clinic at the Singapore National Eye Centre. All subjects underwent a standard examination of dark room gonioscopy and the anterior segment imaging by SS-OCT on the same day. A subset of 29 subjects (23.4%) was imaged bilaterally to assess the differences between eyes.

The Casia SS-1000 Fourier domain anterior segment OCT (Tomey, Nagoya, Japan) that uses 1,310nm wavelength light with a scan speed of 30,000 A-scans per second, was used as the imaging modality to visualize the anterior segment of the eye. We used the 2D angle high-definition (HD) mode of SS-OCT imaging with the (8mm, 8mm) scan dimension. The angle quadrants were graded gonioscopically using the modified Shaffer grading system. Both horizontal and vertical plane scans are completed simultaneously in 0.2 seconds giving four different quadrants of the eye namely: inferior, superior, nasal and temporal scanning.

The dataset of total seven hundred and eight HD SS-OCT images were examined to verify the feasibility of the proposed FD index in angle closure detection. The scleral spur and Schwalbes line angle structures were visible in most nasal and temporal quadrants. Schwalbes line could be detected automatically in 85% of the whole dataset. The experiments are based on each single image, which is labeled as open (3.438 ± 0.497 average grade) or closed (1.036 ± 0.72 average grade) angle by the ophthalmologist.

We evaluated the FD index in comparison with the following biometric angle assessment measurements:

- **mAOD750**: The average of continuous serial AOD measured of every 25μm from 750μm ACA apex point [8].
- **ARA750**: The Triangular area of iridocorneal angle bounded by the angle recess, corneal endothelium and anterior surface of the iris and AOD line typically measured at a point 750μm from the ACA apex point [8].
- **AODsb**: The single AOD measured at Schwalbe's line (SL) [6].
- **ARAsb**: The Triangular area of iridocorneal angle bounded by the angle recess, corneal endothelium and anterior surface of the iris and AODsb line [6].

The comparison of FD index of the iridocorneal angle structure for different quadrant between open and closed angle SS-OCT images using gonioscopic grading as a reference is illustrated in Table I. The mean (σ) FD for open and closed angle were 1.944 (0.045) and 1.894 (0.043), respectively. The FD index is slightly higher (∼0.05) in superior and inferior than nasal and temporal quadrant. Superior and

TABLE I

COMPARISONS OF FD INDEX IN DIFFERENT QUADRANTS FOR OPEN AND CLOSED ANGLE IMAGES.

Quadrant	Open images (n = 472)		Closed images (n = 236)		P value**
	mean (σ)	COV (%)	mean (σ)	COV (%)	
Superior	1.969 (0.046)	2.3	1.918 (0.039)	2.0	<0.0001
Nasal	1.916 (0.048)	2.5	1.860 (0.063)	3.4	<0.0001
Temporal	1.929 (0.044)	2.3	1.881 (0.030)	1.6	<0.0001
Inferior	1.960 (0.041)	2.1	1.918 (0.038)	1.9	<0.0001
Mean	1.944 (0.045)	2.3	1.894 (0.043)	2.2	<0.0001

σ standard deviation, COV coefficient of variation

** Significance level by one sample t-test

TABLE II

PERFORMANCE COMPARISONS OF FD INDEX WITH BIOMETRIC PARAMETERS MEASUREMENT FOR OPEN AND CLOSED ANGLE IMAGES.

Parameters	Open images (n = 472)		Closed images (n = 236)		P value
	mean (σ)	COV (%)	mean (σ)	COV (%)	
FD	**1.944 (0.045)**	**2.3**	**1.894 (0.043)**	**2.2**	<0.0001
mAOD750 (*mm*)	0.413 (0.180)	35.2	0.243 (0.134)	45.6	<0.0001
ARA750 (mm^2)	0.285 (0.102)	35.9	0.168 (0.069)	41.1	<0.0001
AODsb* (*mm*)	0.399 (0.145)	36.3	0.222 (0.105)	47.1	<0.0001
ARAsb* (mm^2)	0.279 (0.098)	35.3	0.165 (0.068)	41.1	<0.0001

FD fractal dimension, AOD angle opening distance, ARA angle recess area, σ standard deviation, COV coefficient of variation

* Measurements were done on Schwalbe's line visible images

inferior quadrant have similar FD index ($\sim$1.96) and nasal and temporal have similar FD index ($\sim$1.92). We observed that the average FD index in open angle was larger than the closed angle glaucoma which shows the higher complexities and irregular form of the open angle ACA geometry.

Table II shows the comparison of FD index with the angle assessment measurements. All the parameters were higher in open than closed angle. However, the coefficients of variance (COVs) of FD index were the lowermost in both open and closed angle images when compared with mAOD750, AODsb, ARA750 and ARAsb, which show the consistency and the stability of FD index. The COVs of mAOD750 and ARA750 were slightly lower than AODsb and ARAsb.

From the above experimental results, the proposed fractal dimension index showed better results in comparison to the angle assessment method. Moreover, the FD index reveals the independent of quadrants while SL based angle assessment could be achieved mostly on nasal and temporal quadrants. Additionally, the FD analysis gives more freedom in computation and is less sensitive to the accurate detection of the Landmarks and it is invariant to rotation, translation and scaling of images. It outperforms the mAOD measurements which are in relation with iris-trabecular contact (ITC), for analyzing qualitatively on the overall region of ITC, SS and SL. Besides, our fractal dimension analysis is performed for each pixel on gray level images that can capture more detailed information of the angle structure. We believe that our findings in this study can serve as a basic grading system for angle closure glaucoma diagnosis in the future.

IV. CONCLUSIONS

We proposed a new strategy to quantify the anterior chamber angle by fractal analysis for detection of open and closed angle SS-OCT images. The fractal analysis is invariant to rotation, translation and scaling and it reveals better performance in comparison with the biometric parameters measurements. Our results suggest that the proposed fractal dimension index (FD index) may be potentially more useful in quantifying ACA for angle closure glaucoma. As a future work, angle assessment method without landmark and unsupervised classification without gonioscopic grading will be our next challenge in detecting angle closure glaucoma.

ACKNOWLEDGMENT

The authors would like to thank Prof. Tin Aung, Dr. Mani Baskaran, Dr. Tin Aung Tun and technicians at Singapore Eye Research Institute for supplying the dataset of SS-OCT images.

REFERENCES

[1] H. A. Quigley, "Glaucoma",. The Lancet, vol. 377, Issue 9774, pp. 1367 - 1377, 2011.

[2] A. Dellaport, "Historical notes on gonioscopy," Surv. Ophthalmol. vol. 20, pp. 137-149, 1975.

[3] T. A. Tun, M. Baskaran, C. Zheng, L. M. Sakata, S. A. Perera, A. S. Chan, D. S. Friedman, C. Y. Cheung, and T. Aung, "Assessment of trabecular meshwork width using swept source optical coherence tomography," Graefes Arch. Clin. Exp. Ophthalmol., vol. 251, pp. 1587-1592, Feb. 2013.

[4] C. J. Pavlin, K. Harasiewicz, and F. Foster, "Ultrasound biomicroscopy of anterior segment structures in normal and glaucomatous eyes," Am. J. Ophthalmol, vol. 113, pp. 381-390, 1992.

[5] H.-T. Wong, M. C. Lim, L. M. Sakata, H. T. Aung, N. Amerasinghe, D. Friedman, and T.Aung, "High-definition optical coherence tomography imaging of the iridocorneal angle of the eye," Arch. Ophthalmol., vol. 127, pp. 256-260, 2009.

[6] J. Tian, P. Marziliano, M. Baskaran, H. T. Wong., and T. Aung, "Automatic anterior chamber angle assessment in hd-oct images," IEEE Trans. Biomedical Engineering, vol. 58, no. 11, pp. 3042-3049, 2011.

[7] C. Cheung, C. Zhen, C. L. Ho, T. A. Tun, R. S. Kumar, F. Sayyad, T. Y. Wong, and T. Aung, "Novel anterior-chamber angle measurement by high-definition optical coherence tomography using the schwalbe line as the landmark," Br. J. Ophtahlmol, vol. 95, pp. 955-959, 2011.

[8] S. N. Ni, J. Tian, P. Marziliano, and H.-T. W. H, "Two new parameters to assess anterior chamber angle for SS-OCT images," in IEEE International Symposium on Biomedical Imaging (ISBI 2013), pp. 1312-1315, 2013.

[9] Y. Xu, J. Liu, N. M. Tan, B. H. Lee, D. W. Wong, M. Baskaran, S. Perera, T. Aung, "Anterior Chamber Angle Classification Using Multiscale Histograms of Oriented Gradients for Glaucoma Subtype Identification," in EMBC 2012, pp. 3167-3170, 2012.

[10] Y. Xu, J. Liu, J. Cheng, B. H. Lee, D. W. Wong, M. Baskaran, S. Perera, T. Aung, "Automated anterior chamber angle localization and glaucoma type classification in OCT images," in EMBC 2013, pp. 7380-7383, 2013.

[11] B. B. Mandelbrot, The Fractal Geometry of Nature (Freeman Press, 1982).

[12] P. Y. Kim, K. M. Iftekharuddin, P. G. Davey, M. Tth, A. Garas, G. Holl and E. A. Essock," Novel Fractal Feature-Based Multiclass Glaucoma Detection and Progression Prediction," IEEE Journal of Biomedical and Health Informatics, vol. 17, no. 2, pp. 269-276, 2013.

[13] N. Otsu, "A threshold selection method from gray-level histograms," IEEE Trans. Systems Man Cybernet vol. 9, pp. 62-66, 1979.

[14] D. Sankar and T. Thomas, "Fractal features based on differential box counting method for the categorization of digital mammograms," In: Journal of Computer Information Systems and Industrial Management Applications, vol. 2, pp. 011-019, 2010.